Department of Physics

University of Crete

Fabrication and characterization 3-D tissue-like phantoms with controllable optical and acoustic properties

Konstantina Epitropaki

Heraklion, June 2017

Table of contents

I. Abstract 3

I. Περίληψη 4

II. Introduction 5

III. Theory 6

i. Light Interactions 6

a. Absorption 7

b. Scattering 9

ii. The Photoacoustic Effect 12

iii. Rheology 14

IV. Materials and Methods 18

i. Instruments 18

a) Spectrophotometer 18

b) Photoacoustic Setup 20

c) Light microscope 23

d) Rheometer 24

ii. Sample Preparation 24

iii. Experimental Process 26

iv. Speed of Sound 28

V. Results 31

i. Absorption-wavelength 31

ii. Speed of Sound – Concentration 36

iii. G' , G''– Frequency 37

VI. Conclusion and Future Work 38

VII. References 40

VIII. Ευχαριστίες 41

I. Abstract

The interest in manufacturing 3D tissue-like phantoms by using different materials has increased dramatically during the last decades. Generally, phantoms can be considered very useful devices either for system calibration or for algorithm optimization. Moreover, tissue equivalent phantoms can be developed with controllable optical, mechanical or even structural properties. Thus, such phantoms can be used as substitutes in order to reduce to a minimum the use of animals during the experimental periods.

The goal of this study is to fabricate homogeneous phantoms that match the optical and mechanical characteristics of tissues in the visible and near-infrared spectral range. In this study, the basic phantom material for phantom manufacturing is PVCP. This material has been purposefully selected since it has been used in previous studies for characterization of absorption, scattering at single and multiple wavelengths and definition of speed of sound. In this project, each sample was measured for its optical absorption using spectrophotometer or wavelengths from 500nm up to 1700nm, for the speed of sound by applying the photoacoustic effect at 5MHz and finally was characterized for its rheological properties by using a rheometer with isothermal frequency scans from 10^{-1} $\frac{rad}{sec}$ to 10^{2} $\frac{rad}{sec}$.

I. Περίληψη

Το ενδιαφέρον για την παρασκευή τρισδιάστατων ομοιωμάτων ιστών από διάφορα υλικά έχει αυξηθεί δραματικά τις τελευταίες δεκαετίες. Γενικά, τα ομοιώματα μπορούν να θεωρηθούν πολύ χρήσιμες συσκευές είτε για βαθμονόμηση συστημάτων ή για βελτίωση αλγορίθμων. Επιπροσθέτως, ομοιώματα ιστών μπορούν να αναπτυχθούν με ελεγχόμενες οπτικές, μηχανικές ακόμα και δομικές ιδιότητες. Συνεπώς αυτά τα ομοιώματα μπορούν να χρησιμοποιηθούν προκειμένου να μειώσουν τη χρήση των ζώων κατά τη διάρκεια πειραματικών περιόδων.

Ο σκοπός αυτής της μελέτης είναι να παρασκευαστούν ομοιογενή ομοιώματα που να ταιριάζουν με τα οπτικά και μηχανικά χαρακτηριστικά του ιστού στην ορατή και υπέρυθρη φασματική περιοχή. Σε αυτήν τη μελέτη, το κύριο υλικό την κατασκευή των ομοιωμάτων είναι το PVCP. Το υλικό αυτό σκόπιμα επιλέχθηκε καθώς έχει χρησιμοποιηθεί σε προηγούμενες μελέτες για τον χαρακτηρισμό απορρόφησης, σκέδασης σε ένα και περισσότερα μήκη κύματος και τον προσδιορισμός της ταχύτητας του ήχου. Σε αυτήν την εργασία, κάθε δείγμα μετρήθηκε για την οπτική απορρόφηση του χρησιμοποιώντας φασματοφωτόμετρο για τα μήκη κύματος 500nmέως 1700nm, για την ταχύτητα του ήχου εφαρμόζοντας το φωτοακουστικό φαινόμενο στα 5 MHzκαι τελικά χαρακτηρίστηκε για τις ρεολογικές του ιδιότητες χρησιμοποιώντας ρεόμετρο με ισοθερμικές σαρώσεις συχνότητας από $10^{-1}\,\frac{rad}{sec}$ έως $10^{2}\,\frac{rad}{sec}$.

II. Introduction

In the last decades, a lot of research has been done regarding tissue simulating phantoms with controllable optical or mechanical properties. In general, the use of tissue equivalent phantoms is considered essential for biomedical imaging since they are utilized not only as calibration standards, but mainly aim to minimize the number of animals employed during experiments. Therefore, it is necessary to fabricate long lasting tissue mimicking phantoms that manage to imitate the realistic geometry, the optical and the mechanical properties of the corresponding tissue type. The previous years, some examples of materials that have been used to develop tissue–equivalent phantoms in biomedical research are intralipid [1], polyacrylamide gels [2], albumin [3], agar [3]and epoxy resin[4][5]. Nowadays, technological achievements offer the opportunity to construct such phantoms in detail using accurate 3D printing.

The optical properties of these materials can be characterized using techniques such as optical spectroscopy, the Kubelka –Munk model [6], Monte Carlo simulations etc. that mainly take into account reflectance and transmittance measurements. On the other hand, in order to determine the mechanical properties of materials, different devices can be used according to the phantom material. More specifically, in case where the sample is hard and thin(up to 1 cm), then it can be measured with a hardness tester, where in cases that the sample is considered soft, rheometric measurements can be performed. Taking into account such measurements, we can obtain information about the material's elasticity, hardness, shear modulus, viscosity etc.

Polyacrylamide gels, agar and albumin phantoms absorb water and therefore are not well suited for experiments that require water contact. Agar and albumin phantoms are also fragile and rapidly degrade over time due to fungal growth and thus have a limited shelf time. Materials such as polyester resin and epoxy resin are popular optical phantoms options, due to their optical transparency and long term stability [7]. However, in contrast to tissue, they have high speed of sound. Polyvinyl alcohol (PVA) is an additional material that suitably combines tissue like optical and acoustic properties, however its preparation involves long freeze-thaw cycles and is sensitive to humidity [8].

In this study, polyvinyl chloride plastisol (PVCP) was used as basic phantom material presenting great advantages, such as stability over time, optical transparency and tissue-like acoustic properties. PVCP is an oil-based liquid insoluble in water that polymerizes and becomes translucent solid when heated to high temperatures (~200^{o}C) and allowed to cool. Initial studies with PVCP have been investigated by Henrichs [9], but a rigorous characterization of material's absorption and reduced scattering were not pursued. Later, Spirou [10] used the same material for phantom fabrication and studied its optical and acoustic properties. In order to control the material's optical properties Black Plastic color (BPC) (M-F Manufacturing Co., Fort Worth, TX, USA) and titanium dioxide (TiO_2) were added as absorber and scatterer respectively. Following studies have been performed to characterize the same material using single or multiply wavelengths laser sources. In 2015 Fonsesca [11] presented a thorough research using PVCP as basic phantom material and studied its optical, acoustic and thermoelastic efficiency of different compositions of PVCP. More specifically, that research was focused on phantom fabrications for Quantitative Photoacoustic Imaging and determination of the speed of sound and acoustic attenuation.

The aim of this work is to fabricate phantoms with tissue equivalent optical and mechanical properties, using the same PVCP material according to previous studies. Each sample was measured for its optical absorption, using spectrophotometric measurements. Finally rheometric and photoacoustic measurements were also performed in order to deprive the material's mechanical properties and delineate the speed of sound.

III. Theory

i. Light Interactions

In this section, the interaction of light with matter and how this causes the phenomena of absorption and scattering will be discussed. The light propagation requires three main concepts that are light emitters, light absorbers and light scatterers. Especially,

the term “light emitters” includes all different mechanisms and processes generating visible light in nature, while light absorbers “sink” part of that visible light. In the last case, it is possible that the absorbed energy to be re-emitted in the form of visible light, like in case of fluorescence.

a. Absorption

The definition “energy absorption” is used to describe the absorption of electromagnetic radiation from a particle. It mentions to the process in which the photons which carry energy and can be absorbed by a particle, for example an atom or molecule. So, absorption is the procedure of light photon energy transfer to an atom or a molecule.

During the phenomenon of absorption, an electron which lies in the ground state of a molecule absorbs a photon of specific energy (that differs accordingly molecules) that equals to the energy difference between the ground and excited state. After that, the electron is transmitted to a vibration level of the excited state [12].

Though, particles can lose energy which they had absorbed either through the exchange of heat or radiation. In nature, at room temperature (~25^{o}C), it can be assumed that most of electrons in the molecule lie in the ground state.

Depending on the absorbed energy, transitions may happen from the ground state to a higher one, always following the quantum selection rules. When the electron is in an excited state, there are several paths that can be followed in order to return to the ground state and the state of minimum energy. Such events can be indicated in the diagram below (Figure 1) and discussed in the following paragraphs.

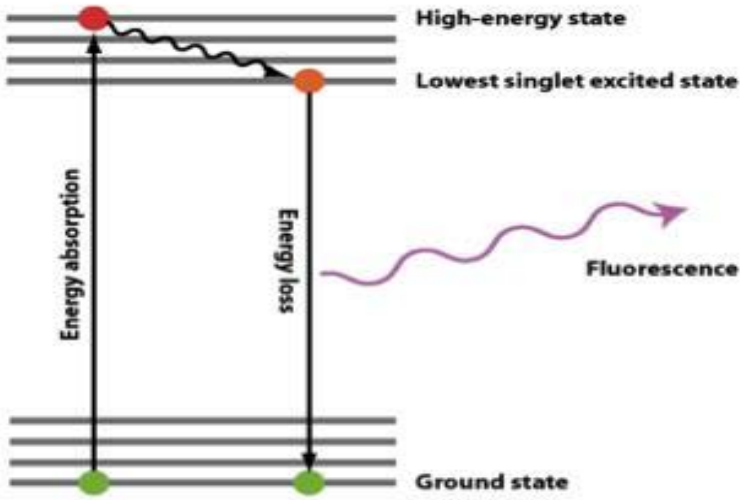

Figure 1: Schematic representation of different light paths of a molecule after absorption of radiation.

Figure 1 depicts a graphical representation of the ensemble of all energy states and the relevant transitions that a molecule can undergo when interacting with light. Moreover, it is showed vibrational and rotational states of electronic state. After absorption of a photon, the system can follow a number of different paths, it means that it can either lose energy via vibrational relaxation reaching the lower vibrational level of the specific excited state or undergo intersystem crossing a triple excited state. From a singlet excited state a photon can relax by radiative emission (fluorescence) to the ground state and similarly from the triplet state it can relax radiative via phosphorescence (will not be discussed here).

Since we have described the basis of absorption, it is obvious that different molecules absorb different energies depending on the configuration of their excited states. As we all know, we consist of 70% water approximately. So, the bigger part of our body is water. The greater absorber in soft tissue, which is the main topic of this study, is hemoglobin (oxyhemoglobin (HbO_2), deoyhemoglobin (Hb)). In Figure 2 the so – called “optical window” (near-infrared (NIR) window) is shown, which describes the area in the near infrared spectrum, where most of the main tissue absorbers (hemoglobin, water, melanin) have the least possible absorption. Near-infrared light (700–2,500 nm) can penetrate biological tissues such as skin and blood more efficiently than visible light because these tissues scatter and absorb less light at longer wavelengths[13].

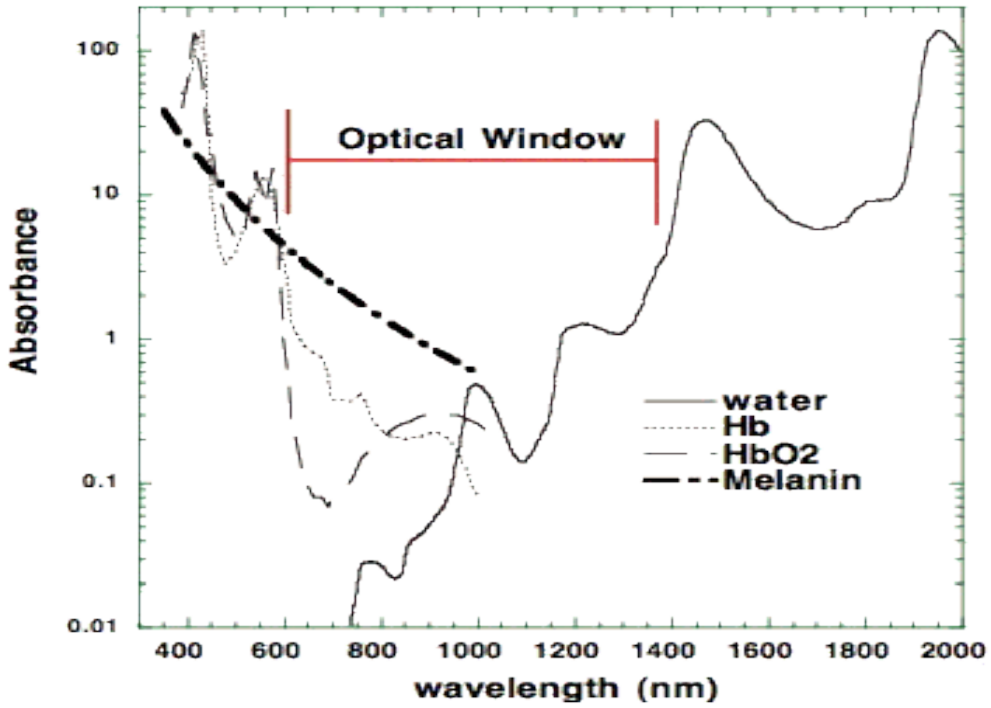

Figure 2:The optical window for tissue imaging, where the absorbance of the main molecules is lower.

b. Scattering

Scattering is a general physical process where some forms of radiation, such as light, sound or moving particles, are forced to deviate from a straight trajectory by one or more paths due to localized non-uniformities in the medium through which they pass. In conventional use, this also includes deviation of reflected radiation from the angle predicted by the law of reflection, as shown in figure 5. Note that in contrary to the absorption, scattering does not comprise re-radiation. Scattering may also refer to particle –particle collisions between molecules, atoms, electrons, photons and other particles.

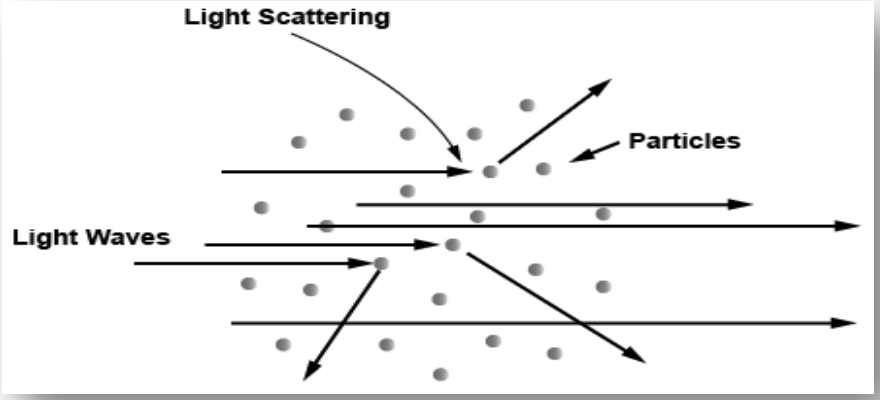

Figure 3: Interaction between light propagating waves and particles during elastic scattering

Optical parameters

In this subsection, the optical parameters which are meaningful for describing and understanding light propagation through samples will be described. These are:

1) Absorption coefficient μ_a: characterizing the absorption properties of a medium.
2) Scattering coefficient μ_s: characterizing the scattering properties of a medium.
3) Scattering anisotropy g: is an indication of transparency of an object.

We know that μ depends on the density (ρ) and atomic number (Z) of a material and the energy (E) of a photon $\mu = f(\rho, Z, E)$. Also, the interaction probability is the sum of probabilities of the different types of interaction, $\mu=\mu_a+\mu_s$.

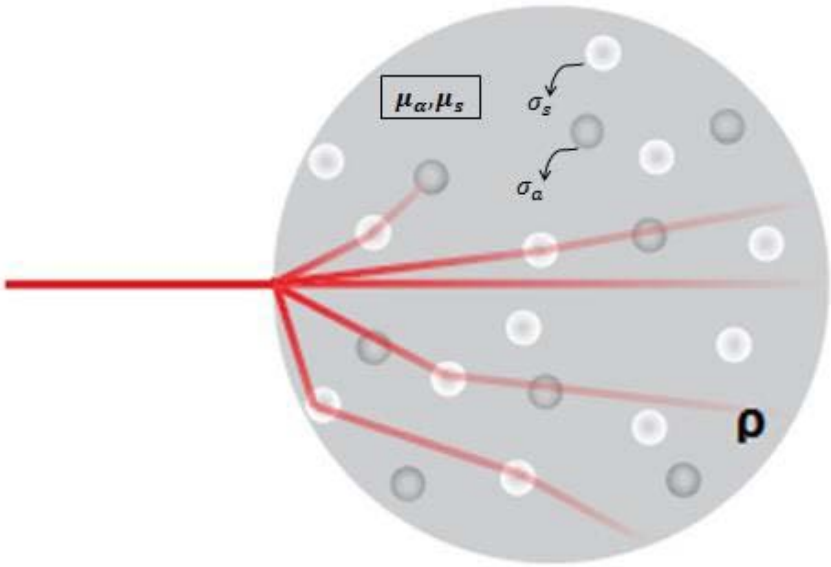

Figure 4: Schematic representation of an ensemble of particles at a density ρ and with absorption and scattering cross-section σ_α , σ_s and absorption and scattering coefficient μ_α , μ_s respectively.

Figure 4 depicts a collection of particles with density ρ and with absorption and scaterring cross sections given by σ_α and σ_ς. In that case, we can write:

$$\mu_\varsigma = \rho\sigma_\varsigma \ (cm^{-1}) \qquad (1) \quad \text{and}$$

$$\mu_\alpha = \rho\sigma_\alpha \ (cm^{-1}) \qquad (2)$$

Consequently, the total macroscopical cross-section μ_t or total attenuation coefficient or transport coefficient can be defined as the probability that a photon gets either scattered or absorbed per unit length. The total attenuation coefficient is given by:

$$\mu_t = \rho\sigma_t = \rho(\sigma_\alpha+\sigma_\varsigma) \qquad (3)$$

whereσ_α, σ_ς, σ_t are the absorption, the scattering ant the attenuation cross-sections respectively, with measurement unit cm^2. The mean free path or scattering mean free path (MFP) can then be defined as:

$$l_\varsigma = \frac{1}{\mu_\varsigma} \ (cm) \qquad (4)$$

which describes the average distance travelled by a moving particle between two scattering events.

In case where the anisotropy of a medium is taken into consideration, the reduced scattering coefficient can be defined as:

$$\mu'_{\varsigma} = \mu_{\varsigma}(1\text{-}g) \quad (cm^{-1}) \qquad (5)$$

In the above equation g is the anisotropy function defining the degree of forward scattering, expressed as a probability function by a Henyey-Greenstein phase function with a coefficient, g. For photon scattering in tissue, g is typically 0.8-1.

Using the reduced scattering coefficient, the transport mean free path (TMFP) can be defined as:

$$l_{tr} = \frac{1}{\mu'_s} = \frac{1}{\mu_s(1-g)} \qquad (6)$$

The TMFP describes the distance that light has to travel until its propagation is completely randomized (diffused). Combing equations (4), (6) it comes up that $l_{\varsigma} = l_{tr}(1\text{-}g)$. The higher the g, the more forward the scattering and the longer it takes for light to become diffuse, resulting in higher penetration distances through samples [14].

ii. The Photoacoustic Effect

Photoacoustic (or optoacoustic) effect is the formation of sound waves following light absorption by a material. The latest years the photoacoustic has been applied in biomedical imaging as well.

In order to generate this phenomenon, high intensity pulsed laser must be delivered to biological tissues. Some of this delivered energy will be absorbed and converted into heat, leading to transient thermoelastic expansion and consequently to wideband (MHz) ultrasonic emission. Afterwards, the generated acoustic waves are detected by

ultrasound transducers. A graphic representation of the photoacoustic principles is depicted in Figure 5.

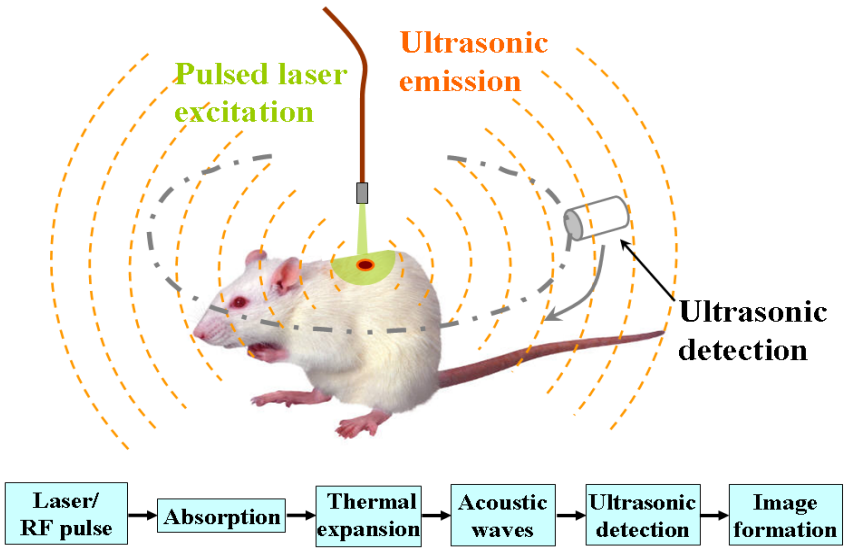

Figure 5: Schematic illustration of basic principles of photoacoustic imaging

.

It is known that absorption is closely associated with physiological properties, such as hemoglobin concentration and oxygen saturation. As a result, the magnitude of ultrasonic emission (i.e. photoacoustic signal), which is proportional to the local energy deposition, reveals physiologically specific optical contrast.

The photoacoustic effect can be described mathematically through the photoacoustic equation:

$$\nabla^2 p(\vec{r},t) - \frac{1}{U_s^2}\frac{\partial^2}{\partial t^2} p(\vec{r},t) = -\frac{\beta}{C_p}\frac{\partial}{\partial t} H(\vec{r},t) \quad (7)$$

where $p(\vec{r},t)$ is the photoacoustic wave pressure in an acoustically homogeneous and non-viscous medium,$U_s$denotes the speed of sound in medium, β is the isobaric volume expansion coefficient in K^{-1}, C_p represents the specific heat in J/(K·kg) and$H(\vec{r},t)$ is a heating function defines as the thermal energy converted in a spatial position $\vec{r}$ and time t by the electromagnetic radiation per unit volume per unit time.For practical calculations, the amount of generated heat by tissues is proportional to the strength of the radiation:

$$H(\vec{r},t) = \mu_\alpha(\vec{r})\Phi(\vec{r},t) \quad (8)$$

where $\mu_\alpha$represents the absorption coefficient andΦ is the optical radiation fluence [15][16].

The equation (7) holds under thermal confinement to ensure that heat conduction is negligible during the laser excitation. The thermal confinement occurs when the laser pulse width is much shorter than the thermal time, therefore no heat is dissipated during excitation. It is obvious from the same equation that the source term is proportional to the first time derivative of heating function, implying thus that the thermoelastic expansion of the medium will give rise to photoacoustic wave propagation only when the heating through the absorption of the incident irradiation changes over time – a constant light intensity would not cause any photoacoustic effect. This explains the reason why pulsed or intensity – modulated lasers resulting in time –variant heating are exclusive employed for this purpose[17].

iii. Rheology

Rheology is the science dealing with deformation and flow of matter. In order to understand this study, it is essential to define the below terms: Shear stress, Shear Rate and Viscosity. Viscosity is a measure of a fluid's resistance to flow. When a fluid starts to flow under the action of a force, a shearing stress arises everywhere in that fluid that tends to oppose the motion. As one layer of the fluid moves past an adjacent layer, the fluid's molecules interact so as to transmit momentum from the fast layer to the slower layer tending to resist the relative motion.

The distinguished feature of a fluid, in contrast to a solid, is the ease with which the fluid may be deformed. If a shearing force, however small, is applied to a fluid, the fluid will move and continue to move as long as the force acts on it. For example, the force of gravity causes water poured from a pitcher to flow, it will continue to flow as long as the pitcher is titled. If the pitcher is turned back up the flow because of the gravitational force is then exactly balanced by pressure force of pitcher wall. Even though a fluid can deform easily under an applied force, the fluid's viscosity creates resistance to this force. Viscosity can be appreciated by visualizing a cube of fluid between two plates as shown in figure 6

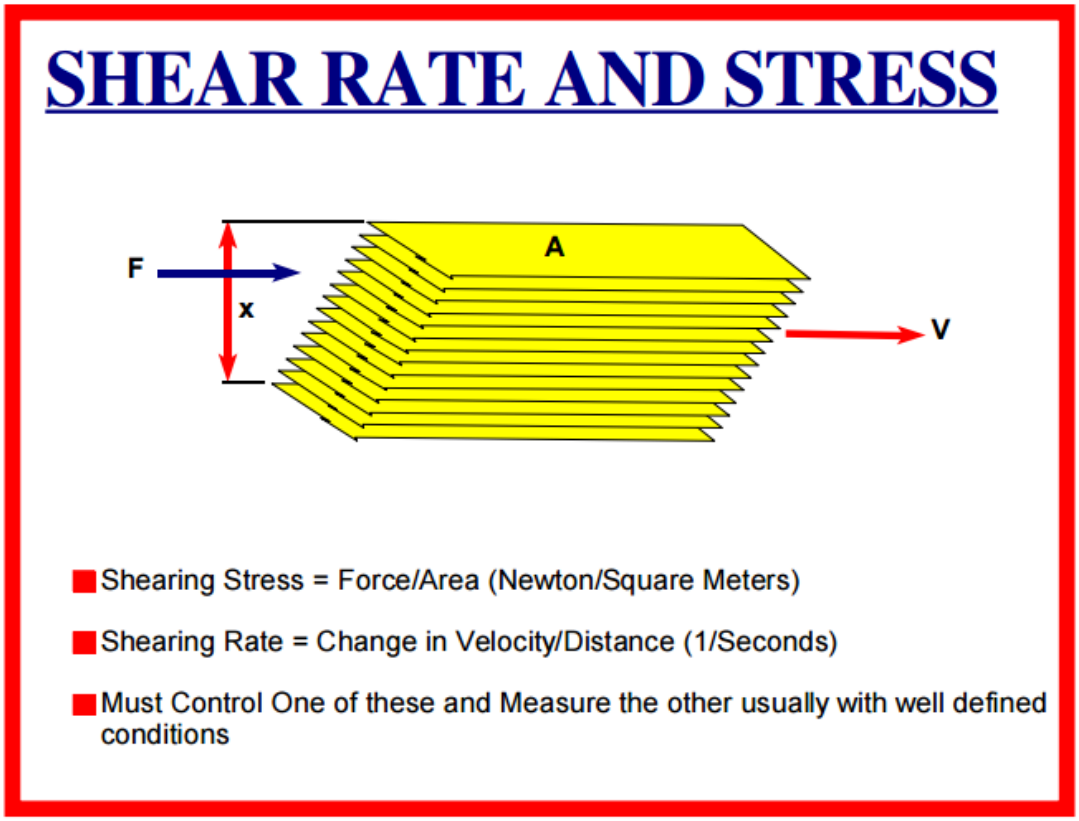

Figure 6: Schematic representation of an applied force to a fluid

If a shearing force (F) is applied to the top plate (A), this plate will move at a specific velocity (V). The layer of fluid immediately below the plate will also move, reaching a velocity almost but not equal to that of plate. In the same way, each successively lower layer of fluid will move at a velocity less than that of its immediate predecessor so that the last layer is almost motionless. The force applied to the top plate divides by the area (A) of the top plate is defined as shear stress and is typically expressed in units of Newton per square meter. The velocity gradient or more commonly, the shear rate is differential change in velocity divided by the distance between the top and bottom plates and is expressed in units of reciprocal seconds. The viscosity of a fluid is derived from these two properties. Viscosity defined as the ratio of shear stress to shear rate.

So, from the above mentioned, we have the below equations:

$$\text{ShearStress} = \frac{\text{Force}}{\text{Area}}\left(\frac{\text{N}}{\text{m}^2}\right) \qquad (9)$$

$$\text{ShearRate} = \frac{\text{ChangeinVelocity}}{\text{Distance}} \ (\text{s}^{-1}) \quad (10)$$

$$\text{Viscosity} = \frac{\text{ShearStress}}{\text{ShearRate}} \ (\frac{\text{N}\cdot\text{s}}{\text{m}^2}) \qquad (11)$$

However, rheology is not only associated with liquids, but also with soft solids or solids which respond with plastic flow rather than deforming elastically in response to an applied force. The term of “plastic flow” means that the deformation of a material that remains rigid under stresses of less than a certain intensity but that behaves under severer stresses approximately as a Newtonian fluid (its viscosity does not change with rate of flow).

In nature, there are also viscoelastic materials like biological tissues such as skeletal bones, articular cartilage, and ligaments [18]. Viscoelasticity is the property of materials that exhibit both viscous and elastic characteristics when undergoing deformation. The term of “elasticity” denotes the ability of a body to resist deforming force and to return to its original size and shape when that force is removed.

The suitable devices in order to measure the viscoelasticity of materials are rheometers. There are two different types of rheometers which are shear (or rotational) rheometers and extensional stress rheometers. The first one controls the applied shear stress, while the others apply extensional stress. The most used rheometers are the shear one and are used for research and development as well as for quality control in the manufacture of a wide range of materials. So, oscillatory rheology is a standard experimental tool for studying the mechanical behavior of soft materials.

When oscillatory shear measurements are performed in the linear viscoelastic material then we obtain information about the elastic response (storage modulusG') and viscous behavior (loss modulusG'') of the tested material. These two modulus are independent of the strain amplitude. In an oscillatory shear experiment the sample is placed between two plates as shown in figure 9(a). While the top plate remains stationary, a motor rotates the bottom plate, so the sample is exposed to a sinusoidal strain (γ) at an angular frequency of ω will respond with a gradual approach to a steady sinusoidal stress (σ)

$$\gamma = \gamma_o \sin(\omega t) (12)$$

$$\sigma(t) = \gamma_o (G'(\omega) sin\omega t + G''(\omega) \cos(\omega t)) (13)$$

Thus, from equations (12),(13) we can find the storage modulusG' (elastic response), loss modulusG''(viscous behavior). As shown the figure 9 (b), if the tested material is an ideal solid, then the sample stress is proportional deformation and the proportionality constant is the shear modulus of the material. The stress is always in phase with the applied sinusoidal strain deformation. In contrast, if the material is a purely viscous fluid, the stress in the sample is proportional to the rate of strain deformation, where the proportional constant is the viscosity of the fluid. The applied strain and the measure stress are out of phase, with a phase angle δ=π/2. However the viscoelastic materials show that contains both in-phase and out-phase contributions, as depicted in the bottom graph of figure 9 (b); these contributions reveal the extents of solid –like (red line) and liquid –like (blue dotted line) behavior. Consequently the total stress response (purple line) shows a phase shift δ with respect to the applied strain deformation, that lies between that of solids and liquids, 0<δ<π/2[19].

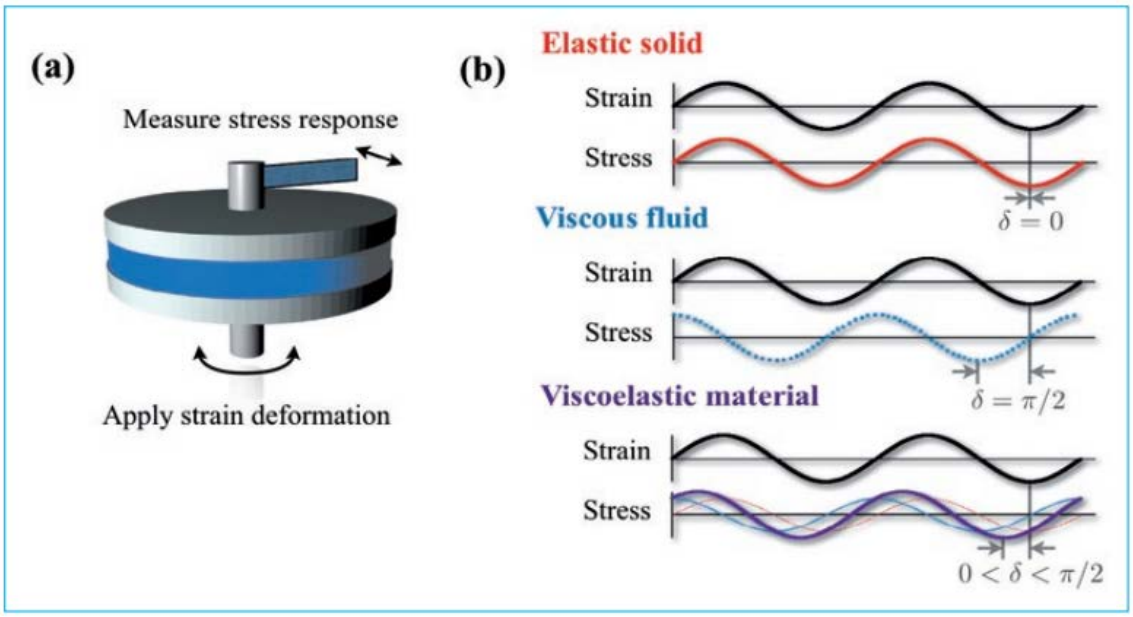

Figure 9:(a) Schematic representation of a typical rheometry setup, with the sample placed between two plates.(b) Schematic stress response to oscillatory strain deformation for an elastic solid, a viscous fluid and a viscoelastic material.

IV. Materials and Methods

In this chapter, the instruments used, the sample preparation and the experimental procedure will be discussed. More specifically, quantitative absorption measurements of a material as a function of wavelength were performed via a spectrophotometer. In addition, a hybrid photoacoustic setup was also used in order to define the time of light required between the photoacoustic effect in a sample and the detection from an ultrasound transducer. Moreover, a light microscope helped in measuring, the thickness of each sample prior each measurement and a rheometer, provided information about the viscoelasticity of the tested material as a function of frequency.

i. Instruments

a) Spectrophotometer

Spectrophotometer absorbance, transmittance and reflectance measurements as a function of the wavelength are used in order to deprive information about material's optical properties.

In this experiment, Lamda 650 Spectrophotometer was used. As shown in Figure 6, two radiation sources, a deuterium lamp and a halogen lamp, cover the working wavelength range of the spectrophotometer. For operation in near infrared and visible ranges, the range was our samples were measured, source mirror M1 reflects the radiation from the halogen lamp onto mirror M2. At the same time it blocks the radiation from the deuterium lamp. The radiation is reflected from mirror M2 via mirror M3 through an optical filter on the filter assembly to mirror M4.

From mirror M4 the radiation is collimated at mirror M5 and reflected to the grating table G1. It is dispersed at the grating to produce a spectrum. The rotational position of the grading effectively selects a segment, reflecting this segment to mirror M5 and then it guided to mirror M6.The radiation is reflected via mirror M6 to the grating on grating table G2 and then via mirror M6 to mirror M7. The rotational position of

grading table G2 is synchronized to that of G1. All slits are located on the slit assembly which is put among mirrors M6 and M7. Moreover, a common beam mask is mounted between the slit assembly and mirror M7.

From mirror M7 the radiation beam is reflected via toroid mirror M8 to the chopper assembly. As the chopper assembly rotates, a mirror segment, a window segment and two dark segments are brought alternately into the radiation beam.

When a window segment enters the beam, radiation passes through to mirror M9 and is then reflected via mirror M10 to create the reference beam. When a mirror segment enters the beam the radiation is reflected via mirror M10′ to form the sample beam. When a dark segment is in the beam, no radiation reaches the detector, permitting the detector to create the dark signal.

The radiation passing alternately through the sample and reference beam reflected by mirrors M11, M12, M13, M11′, M12′, M13′, respectively of the optics in the detector assembly onto the appropriate detector. The beams are combined directly on the light –sensitive layer of the detector. Mirror M14 is rotated to select the required detector. A photomultiplier is used in the UV/Vis range while a lead sulfide detector is used in the NIR range.

Essentially, the principle of spectrophotometer is based on the Beer – Lambert Law which relates the attenuation of the light to the properties of the material through which the light is travelling. For each wavelength of light passing through the spectrophotometer, the intensity I_0 of the light passing through the reference cell is measured. The intensity $I_1$of the light passing through cell is also measured for that wavelength and is less than I_0as the sample absorbs some of the light. The absorbance (A) is defined via the incident intensity $I_0$and transmitted $I_1$by

$$A = \log_{10}\left(\frac{I_1}{I_0}\right) = \varepsilon c l \quad (14).$$

According to equation 14, the absorption (A) is proportional to constant ε, represents the molar extinction coefficient, c denotes the concentration of the sample and l, is the thickness of the sample.

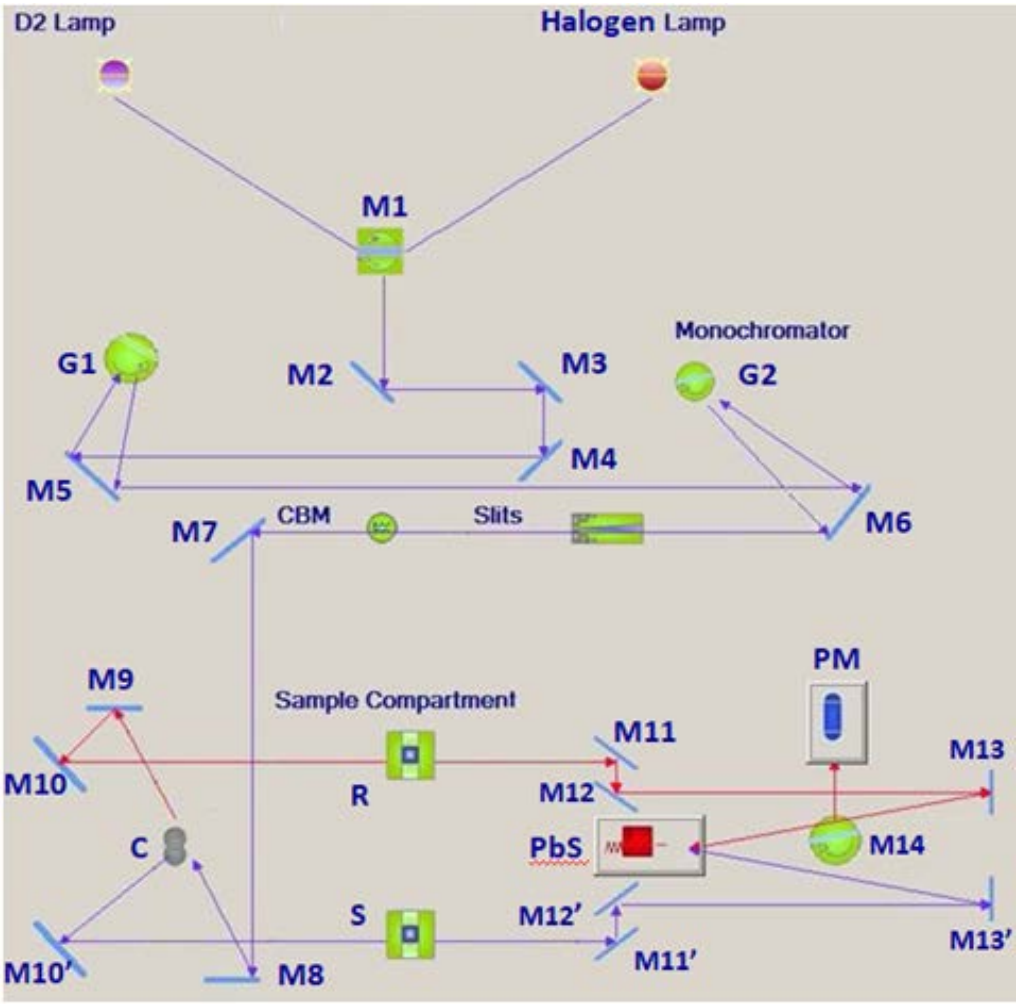

Figure 6: The optical system of spectrophotometer. M, mirror; G, grating table'; CBM, common beam mask; C, chopper; R, reference beam; S, sample beam; PbS, polycrystalline lead sulfide detector; PM, photomultiplier.

b) Photoacoustic Setup

Figure 7 depicts the photoacoustic setup used in order to measure the time of light between the effect and the acoustic detection of the propagated signal. The setup consists of a diode pumped nanosecond laser source (QIR-1064-200-S, CrystaLaser LC, Reno, NV, USA) emitting at 1064 nm in IR with 10 ns pulse width and 6.8 kHz repetition rate. The laser beam is focused on a Lithium Triborate (LBO) second harmonic generation crystal (Castech Inc, Fuzhou, China) in order to get a visible wavelength at 532 nm. This wavelength was specifically selected for effective

photoacoustic signal excitation due to its intense absorption by the biological specimens (melanin, hemoglobin). Subsequently, the beam passes through a second lens to form a telescopic configuration which expands the beam approximately two times.

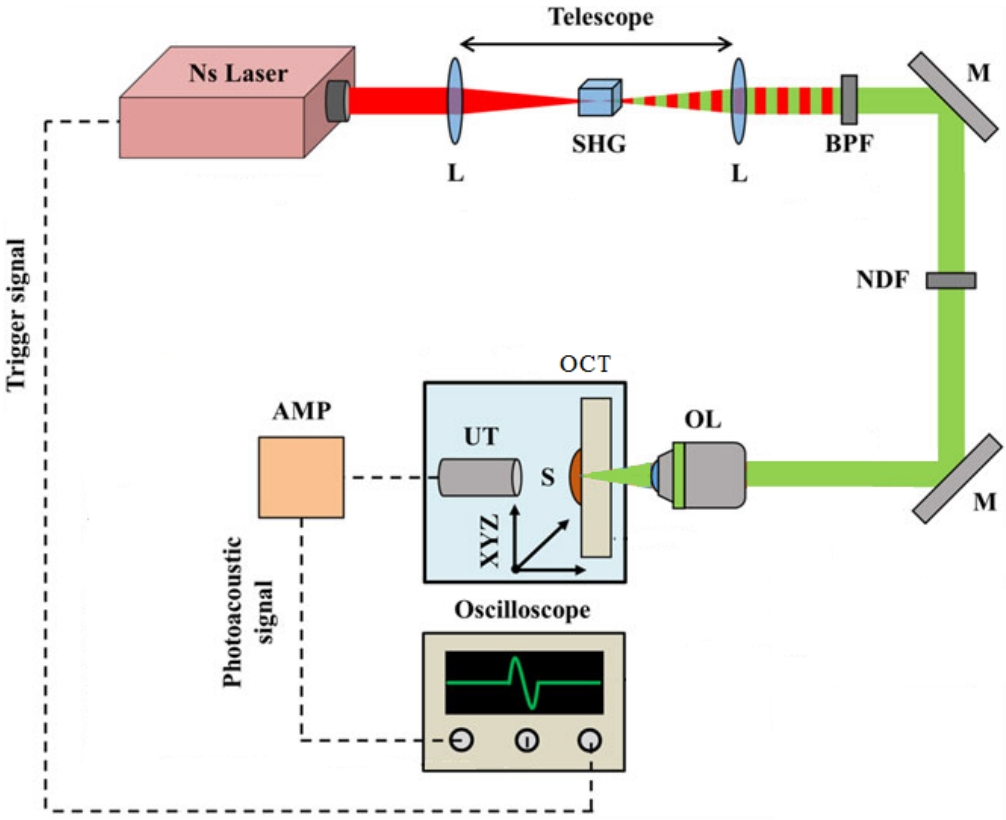

Figure 7: Scheme of the photoacoustic setup. L, lens; M, mirror; SHG, second harmonic generation crystal; BPF, band-pass filter; NDF, neutral density filter; OL objective lens; OCT, optical clear tank; S, specimen; XYZ, motorized XY and manual Z stages; UT, ultrasonic transducer; AMP, amplifier.

A bandpass filter (FF01-531/40-25, Semrock, Rochester, NY, USA), permitting only the visible wavelength transmission (from 511 to 551 nm), is subsequently placed to cut off the residual fundamental light. A number of neutral density filters is also placed in order to attenuate the laser beam energy at the focal plane and prevent the potential damage of the sample. Finally, using a couple of high reflection mirrors, the beam is guided into a properly modified inverted optical microscope (Labovert, Leitz,Wetzlar, Germany).

An objective lens with 0.2 numerical aperture (NA) is placed to focus the beam tightly onto the sample. The specimen is placed at the bottom of an optically clear tank and the last is fixed into a circular basis (Figure 8). The positioning of the sample is performed by two μm resolution XY motorized stages and the z-axis movement is controlled manually using the microscope.

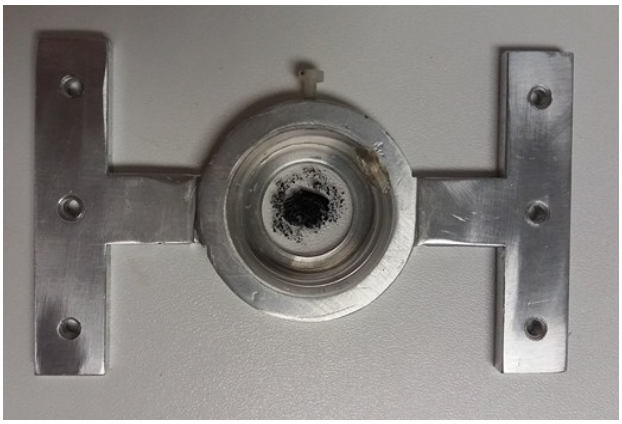

Figure 8: Picture of the circular basis placed on the inverted microscope.

At the superior side of the sample an ultrasonic transducer, with central frequency 5 of MHz is placed in a confocal and coaxial configuration with respect to the illumination focus. The detected ultrasound signals are subsequently amplified using a low noise RF amplifier (AU-1291, Miteq, NY, USA; gain 63dB) and recorded via a speed high oscilloscope (DSO7034A, Agilent Technologies, Santa Clara, CA, USA; bandwidth: 350 MHz, sample rate: 2 GSa s–1). Finally, the acquisition onset of the time – domain photoacoustic signal is triggered internally by the control unit of nanosecond laser source.

By using this method, the time required in order photoacoustic signal to propagate through the samples was measured. Due to the fact that the tested samples are optically transparent, we painted the bottom of each specimen with black

pigment(black line at the bottom of specimen) in order to absorb the laser energy as shown in figure 9.

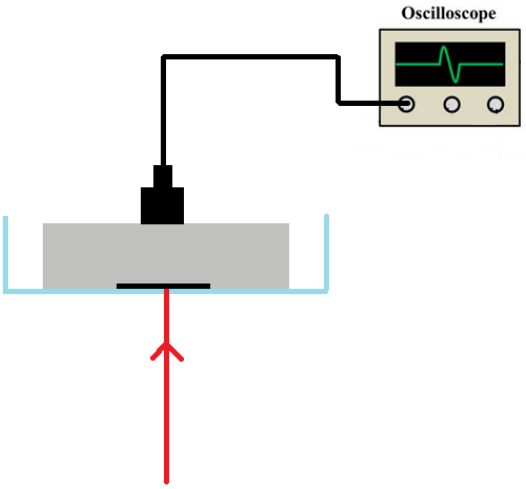

Figure 9: Schematic representation of the measuring process. The laser beam (red line)incidents the black spot lying on the bottom of the specimen (grey area), where the photoacoustic effect occurs. Later the ultrasound transducer detects the photoacoustic signal recorded by an oscilloscope.

c) Light microscope

In order to measure the thickness of each specimen, we used Leica DM RM microscope. Before thickness measurements were performed, a calibration process was followed. Initially, a glass object of known thickness 3 mm was measured. Since the calibration standard was optically clear, the first step of the process was to focus on its upper surface. Afterwards, we measured the number of the revolutions (revs) that the manual z axis stage had to complete, in order to focus on the bottom surface of the standard. We found out that 9 revs were required to do so. Taking into account this information, the micrometric distance that the stage travels per each revolution was calculated up to 330 μm. Consequently, the samples were measured by following the same process. More specifically, the upper surface of each sample was initially focused. Afterwards, we measured how many revs were required to observe clearly the bottom surface. So, the thickness d was calculated by equation (15):

$$d = revs \cdot 330\ (mm) \qquad (15)$$

In addition, it was assumed that the reflective index of glass (n=1.45) and PVCP (n=1.43)[20]were approximately the same at room temperature.

d) Rheometer

In order to characterize the PVCP phantoms for its mechanical properties, an ARES (Advanced Rheometric Expansion system) 100 FRTN1 strain-controlled rheometer (TA instruments) was used. It consists of parallel plate geometry which has diameter 25 mm. A strain amplitude dependence of the complex shear modulus at ω=100 $\frac{rad}{sec}$ and 10 $\frac{rad}{sec}$was applied which determined the viscoelastic regimes of the tested materials. In addition, measurements involved isothermal frequency scans in the range of $10^{-1} < \omega < 10^{2}$ $\frac{rad}{sec}$.

ii. Sample Preparation

The manufacturing of PVCP phantoms was mainly based on a protocol described by Bohndiek [22].

Materials

The materials used, are described in detail in the following list:

- Polyvinyl Chloride Plastisol (PVCP; M-F Manufacturing Co., Fort Worth, TX, USA)
- Green Plastic Color (GPC; M-F Manufacturing Co., Fort Worth, TX, USA)
- Red Plastic Color (RPC; M-F Manufacturing Co., Fort Worth, TX, USA)
- Blue Plastic Color (BLPC; M-F Manufacturing Co., Fort Worth, TX, USA)
- Yellow Plastic Color (YPC; M-F Manufacturing Co., Fort Worth, TX, USA)
- Black Plastic Color (BPC; M-F Manufacturing Co., Fort Worth, TX, USA)
- Soft Plastisol (SP; M-F Manufacturing Co., Fort Worth, TX, USA)
- Circular Aluminum Mold (resistant to temperatures over 180^{o}C)
- Heat proof gloves
- C clamp

- 100 mL round bottom flask
- 300 mL crystallization dish
- Engine Oil
- Stirrer plate with magnetic stirrer bar
- Thermometer
- Vacuum line
- Fume hood

Procedure

The first step of the sample preparation is to place a crystallization dish filled with engine oil on a heated stirrer plate. It must be noted that the whole process takes place in a fume hood. After we mix the desired quantities of PVCP with softeners or colors, we pour the solution into 100 mL capacity round bottom flask and add a magnetic stirrer bar.

The flask must be stabilized with a C clamp so that the bottom of flask does not touch the bottom of crystallization dish but the solution is externally covered by the engine oil. In addition, the flask must be connected with a vacuum line with a valve to permit the fumes to evaporate, and verify that the air bubbles added in the mixture stirring are disappeared. A thermometer is placed into the engine oil in order to check the temperature every time. After this assembly, we are ready to start the sample manufacturing. We turn on the heated stirrer plate with set point at 200^{o}C, begin stirring and open the vacuum line in order to eliminate air small bubbles that are observed. We, also, put the mold on the stirrer plate to be heated. Then, we wait until the temperature of the solution reaches at 200^{o}C. When the temperature is around 130^{o}C, the material will become viscous and when it is close to 180^{o}C the phase transition is completed. By the time the temperature reached up to 200^{o}C, we turn off the heated plate, the stirring and release the vacuum.

Afterwards, we remove the flask from the crystallization dish with engine oil. Immediately, we pour the solution into the heated mold. Finally, we allow the material to set for a few hours and then the phantom is ready for use.

This process lasts approximately 40 minutes. A picture of the experimental set up is shown in Figure 10.

Figure 11: Picture of the sample preparation setup.

iii. Experimental Process

In this project, many PVCP phantoms were fabricated with different quantities of PVCP, colors and different softener concentrations. Firstly, colored specimens (Figure 11) were manufactured with thick approximately 2mm and are measured in a spectrophotometer for their absorption in a regime ranging from 500nm to 1700nm. For each color three different samples were fabricated three times and were measured in three different locations in order to verify the homogeneity of the sample. In the table below (Table 1), the characteristics of the samples produces are presented.

Figure 11: Picture of the colored samples with an approximate thickness of 2mm.

Sample	PVCP (gr)	Pigment (gr)	Total (gr)	Thickness (mm)	Concentration (%w/w)
Green	4.9841	0.0317	5.0158	2.310	0.6
Red	4.9828	0.0296	5.0124	2.310	0.6
Blue	4.9918	0.0350	5.0268	2.310	0.6
Yellow	4.9915	0.0287	5.0202	2.310	0.6
Black	4.9858	0.0325	5.0183	2.310	0.6

Table 1: Quantities of colored samples for optical measurements.

A second series of sample preparation involved the manufacturing of optically transparent samples using PVCP and a compatible softener. For rheological and optical measurements, specimens were prepared with a thickness around 2 mm while for photoacoustic measurements their thickness leveled up to approximately 6 mm. These samples were manufactured according to the quantities shown in Table 2 and Table 3 respectively.

Sample	PVCP (gr)	Softener (gr)	Total (gr)	Thickness (mm)	Softener Concentration (w/w %)
1	5.0151	0	5.0151	2.310	0
2	4.5358	0.5190	5.0548	2.475	10
3	4.0634	1.0059	5.0693	2.475	20
4	3.5150	1.5080	5.0230	2.310	30

Table 2: Quantities of transparent samples for optical and rheological measurements.

Sample	PVCP (gr)	Softener (gr)	Total (gr)	Thickness (mm)	Softener Concentration (w/w %)
1	12.5258	0	12.5258	5.775	0
2	11.2819	1.2618	12.5437	5.775	10
3	9.9996	2.5167	12.5163	5.775	20
4	8.7571	3.7550	12.5121	5.775	30

Table 3: Quantities of transparent samples for photoacoustic measurements.

As described above, the thickness measurements were performed using an optical microscope for better accuracy, since the soft nature of the material did not allow the measurement via a caliper.

iv. Speed of Sound

In order to define the speed of sound of the tested materials, equation (16) was used (15) :

$$U = \frac{d}{t}\left(\frac{m}{s}\right) \quad (16)$$

where U represents the speed of sound of sample, d is the thickness of sample and t denotes the time which the photoacoustic signal need to propagate through the sample and reach the upper surface to be detected by ultrasound transducer.

As describes previously, the speed of sound of each material was calculated by using a photoacoustic setup. More specifically, to generate photoacoustic signal a pulsed laser beam incidents the specimen. Some of this delivered energy was absorbed from the black pigment placed at the bottom of each sample and partially converted into heat. Then, a transient thermoelastic expansion occurred and acoustic waves were generated. The photoacoustic signal was collected by an ultrasound transducer connected to an oscilloscope, a typical example of which is shown in Figure 12. As depicted in Figure 13, the x axis represents time in μsec units. The estimated time is calculated by modifying the divisions of the oscilloscope accordingly so as the first division meets the first peak of the observed signal.

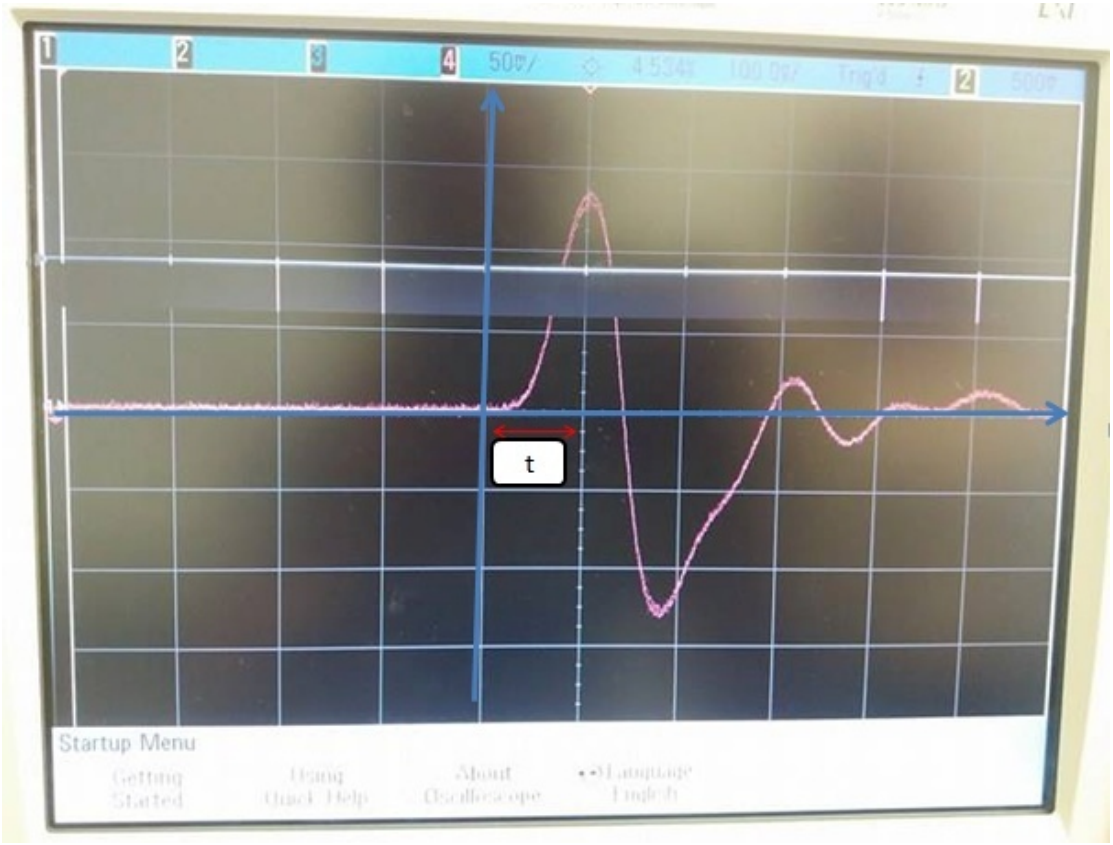

Figure 12:Typical photoacoustic signal from a PVCP phantom.

In Table 4, the thickness d, the time t and the speed of sound U of each tested specimen are represented. Note that these samples were manufactures according to the described in Table 3.

Sample	d (mm)	t(μsec)	U(m/s)	Concentration (w/w %)
1	5.775	4.12	1402	0
2	5.775	4.12	1402	10
3	5.775	4.03	1433	20
4	5.775	3.96	1458	30

Table 4: The thickness d, the time t and speed of sound of the measured samples.

To calculate the experimental error of this process we took into account a few parameters. More specifically, to calculate the error of each thickness measurement resolution of the optical microscope as well as the resolution of our eye was considered. Regarding the resolution of the eye since we could not distinguish where exactly the bottom surface was focused. The error was estimated to rev, meaning approximately 150 μm (1 rev ~ 330 μm).

The resolution of optical microscope is given from equation (17):

$$resolution = \frac{\lambda}{2NA} (17)$$

where λ=0.55μm for visible light and NA =0.12 represents the numerical aperture of the objective lens. Thus, the error of thickness is calculated:

$$\delta d = \sqrt{(resolution\ of\ upper\ surface)^2 + (resolution\ of\ bottom\ surface)^2 + (half\ rev)^2} \quad (18)$$

To evaluate the error of the time measurement the repetition rate of the pulsed laser was taken into consideration. The frequency was f = 5MHz, therefore the period T (1/f) was 200nsec. Thus, the error in time is δT=T/2, where δT was divided by 2 due to diffraction limit of Airy disks.

Finally, the error propagation of speed of sound is given from the following equation

$$\delta U = U\sqrt{\left(\frac{\delta d}{d}\right)^2 + \left(\frac{\delta t}{t}\right)^2} \quad (17)$$

In Table 5, the speed of sound and the respective errors are shown.

Sample	Concentration (w/w %)	U(m/s)	δU(m/s)
1	0	1402	50
2	10	1402	50
3	20	1433	51
4	30	1458	53

Table 5: The speed of sound with error of each sample.

V. Results

In this section, the results of this study will be presented and discussed. Firstly, the diagrams of absorption as function the wavelength are depicted, following the diagram with speed of sound as function the concentration and finally the diagrams with G´ (elastic modulus) as function the frequency are shown.

i. Absorption-wavelength

In the following diagram, the absorption spectrum as a function of the wavelength of a sample consisted only from clear PVCP (clear) is shown in Figure 13.

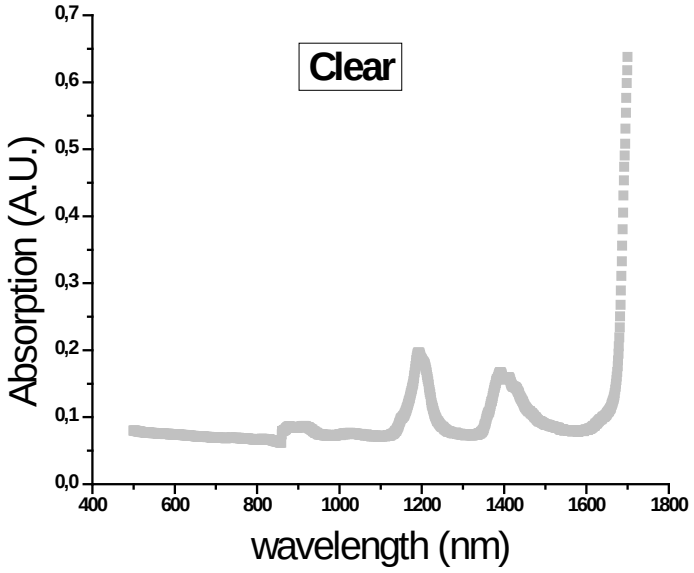

Figure 13: Absorption spectra of clear sample as a function of the wavelength.

PVCP itself in not absorbing but appears prominent absorption peaks at 910, 1190,1400 and 1720 nm, most likely representative of vibrational energy transitions in PVC. It should be noted that the intrinsic absorption may vary to a certain extent with the sample preparation process, including heating rate and final heating temperature, therefore standardized preparation of the materials is advised [10][21]. From the above diagram (Fig. 13) , it is clear that the PVCP indeed appears the expected peaks.

In the following Figures, the absorption spectra of colored samples are depicted. More specifically, these specimens were produced by mixing green, red, blue and yellow colors compatible with clear PVCP material.

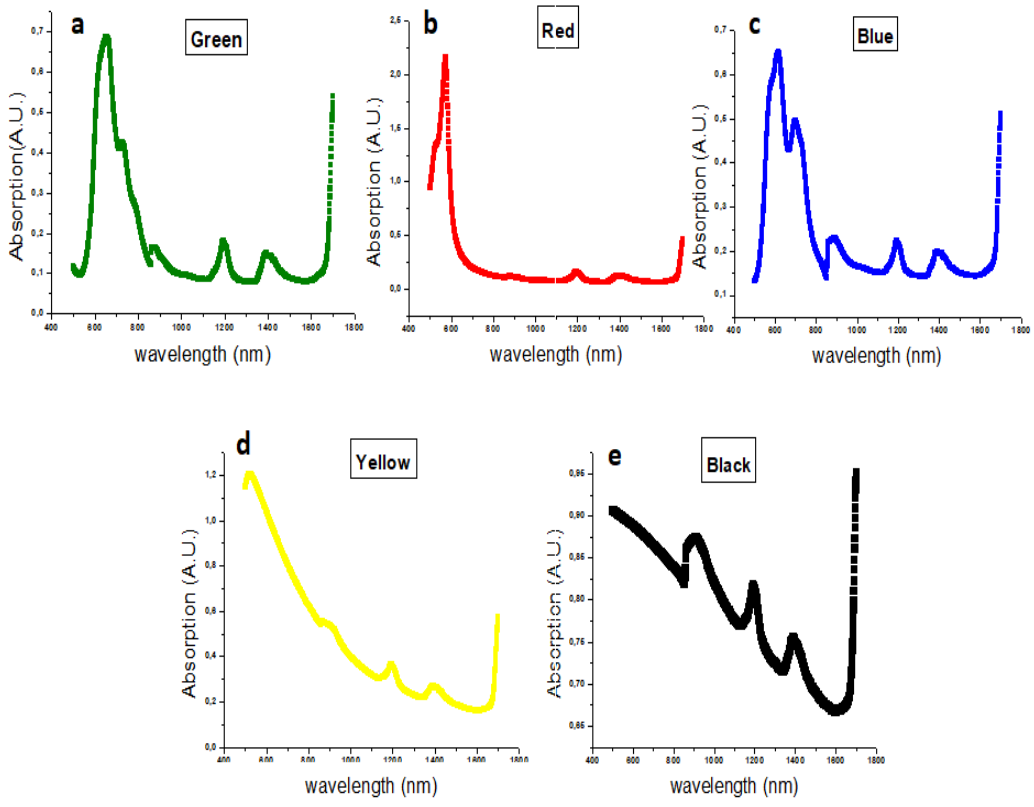

Figures 14 (a- e): Absorption spectra of colored samples as a function of the wavelength. The added colors were green, red, blue, yellow and black respectively.

The main outcome by observing these spectra lies on the fact that the three typical peaks are consistently present at 910, 1190 and 1400 nm, which brings into assumption that they can be considered characteristic of the behavior of PVCP

material itself. In addition, in each diagram the behavior of each color is observed. In Figure 19 a common graph of the measured absorption spectra is presented.

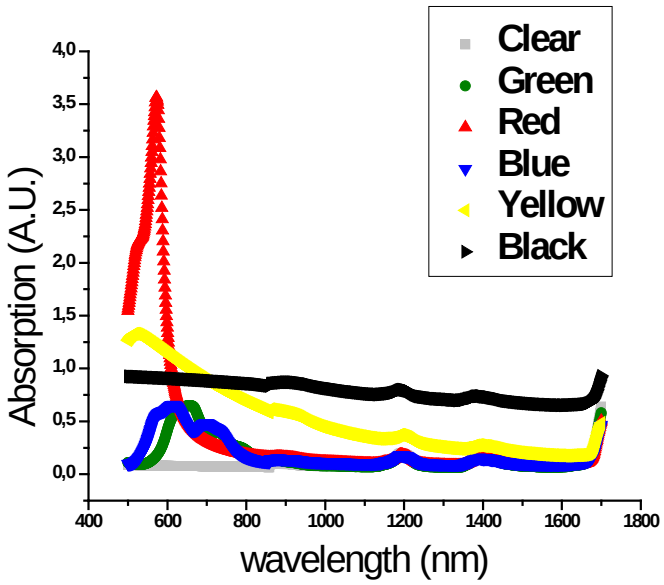

Figure 15: Absorption spectra of colored and clear samples as function wavelength.

In order to clarify if the absorption peaks observed occurs due to the mixing of the pigments with clear PVCP or by the pigments themselves, we diluted 1 drop of each color in ethanol that is considered a great dissolver. The mixture pigment – ethanol was placed in a plastic cuvette and measured for absorption in a spectrophotometer. In the table bellow (Table 6), the quantities of each color and the ethanol in which they are diluted, is shown.

Sample	Pigment (gr)	Ethanol (gr)	Total (gr)
Green	0.02645	10.16955	10.19600
Red	0.2753	11.42947	11.45700
Blue	0.02963	10.30257	10.33220
Yellow	0.02690	11.1021	11.12900
Black	0.03125	10.52025	10.55150

Table 6: Quantities of diluted colors in ethanol.

Apart from the previous cuvettes, another one was measured which containing only ethanol, the absorption values of which were later removed from the colored cuvette values. Their absorption spectra are shown in the following Figures (Fig 16 (a-e)).

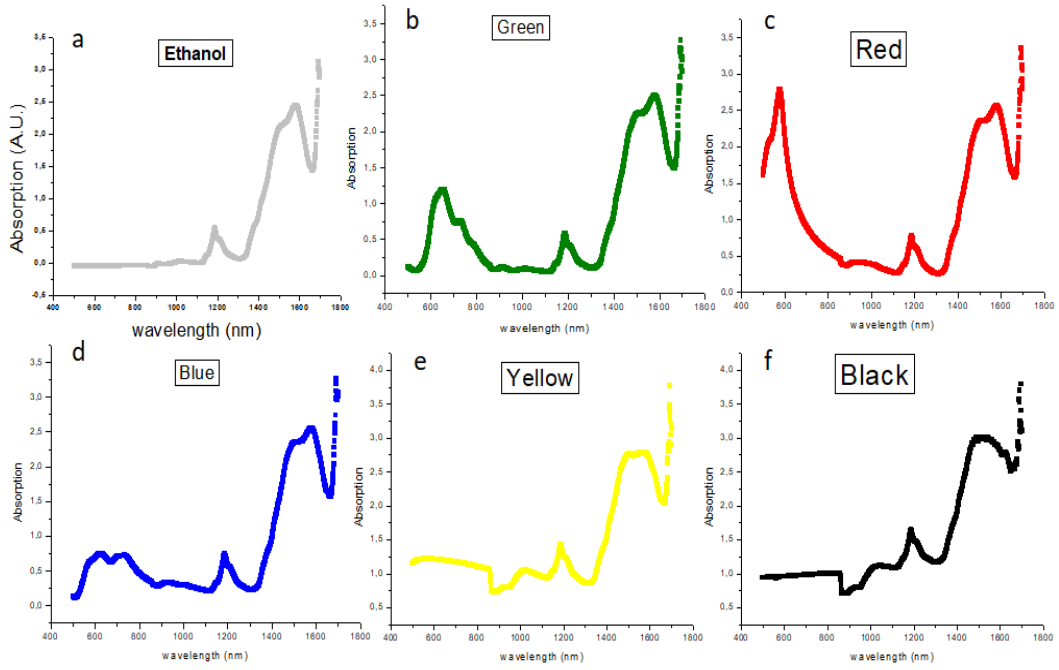

Figure 16 (a – e): Absorption spectra of clear ethanol and colors as function wavelength.

From the above diagrams, the characteristic spectra of ethanol as well as the ones for each colored sample are depicted that denote the same behavior as the samples measured previously (Figures 16 a - e).

Following, a third series of experiments included the fabrication of samples with different softener concentration. These samples were also measured with the spectrophotometer from 500nm to 1700nm for their absorption.

The first assumption is that since no additional pigment was added, but only softener, no significant changes should be observed in these spectra. Indeed, the Figures below (Figure 17 a - e) confirm the initial hypothesis where the absorption spectrum of each sample with different softener concentration is depicted. The Figure 18 shows that as adding softener the optical properties are unchangeable.

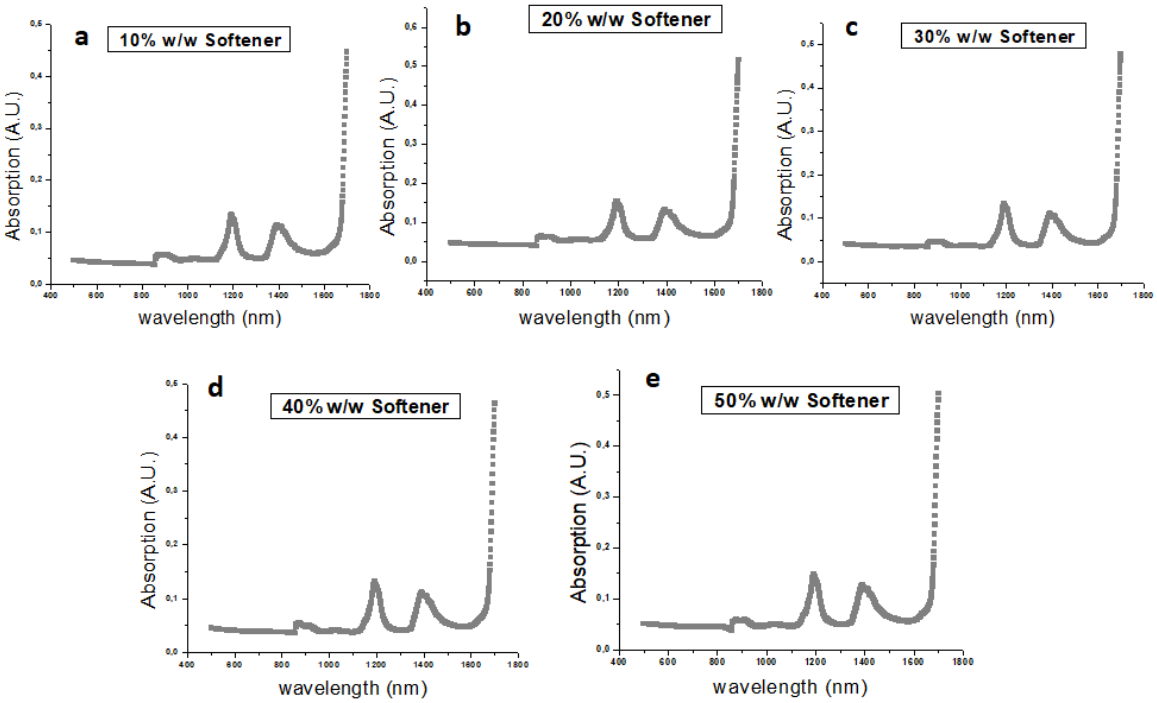

Figures 17 (a – e): Absorption spectra of soft samples as function wavelength.

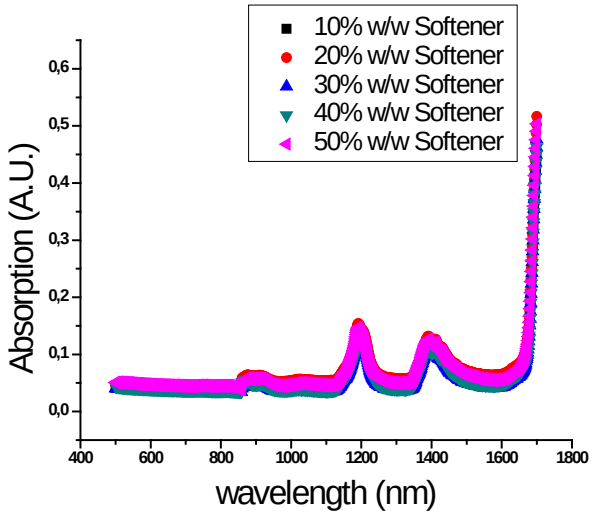

Figure 18: Absorption spectra of all soft samples as function wavelength. The optical properties do not change by softener adding.

ii. Speed of Sound – Concentration

The below figure (Figure 19) represents the speed of sound of each tested specimen as a function of its concentration. As the concentration of the softener increases, the samples become softer

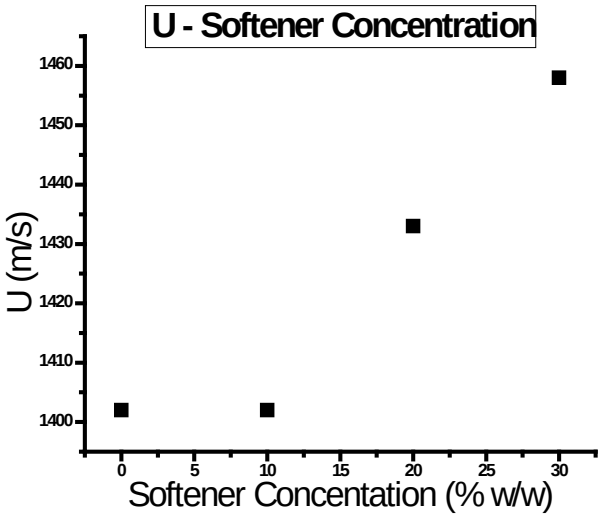

Figure 19: Speed of sound for PVCP samples with various levels of softness.

Figure 18 depicts the speed of sound of PVCP at 5 MHz. It is obvious that the speed of sound increases slightly as the concentration of softener increases as well.

In previous study, Fonesca et al [11] used the same PVCP material with harder addition. The results of this work proved that by adding hardener at the basic material, the speed of sound increased also. Therefore, our initial hypothesis in our study was that by increasing the softener concentration, the speed of sound would probably decrease. The experimental results, on the other hand, showed that by adding more softener in our basic PVCP material, the speed of sound increased, which was considered rather unexpected. An assumption of why this phenomenon appeared is that the PVCP consists of macromolecule chains. In this case, the softener addition possibly creates small liquid channels between them, thus wave probably propagates faster through them.

iii. G' , G"– Frequency

In this study, an attempt was made for characterization of PVCP's rheological measurements. The diagrams below represent the G΄ and G΄΄ terms as a function of the frequency. The samples were prepared with different softener concentration, where the exact quantities of each material are shown in detail in Table 4.

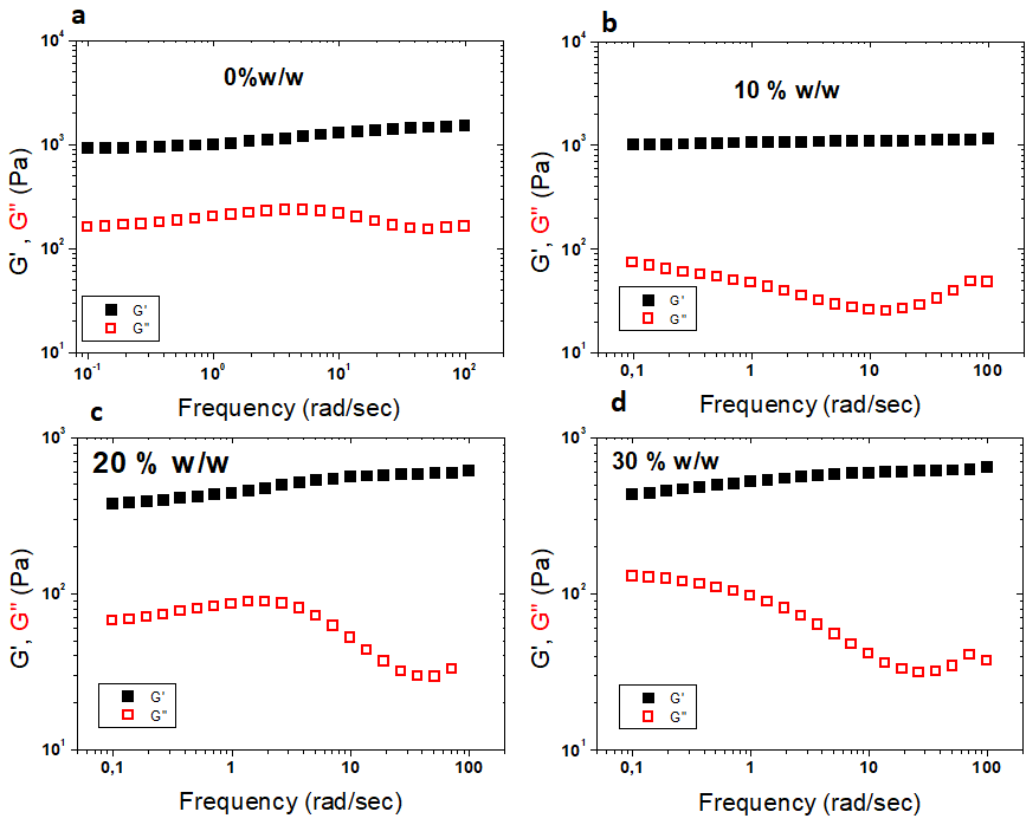

Figure 20 (a– d): G΄, G΄΄ as function of the frequency in samples with different softener concentration.

A first remark on the above figures is the fact that PVCP material behaves as a solid – elastic since in all cases G΄presents bigger values than G΄΄.

In addition, it is clear that the G΄reduces as the concentration of softener increases. Moreover, it seems that G΄does not have a strong dependence on the frequency, which phenomenon is stronger in higher frequencies, therefore it can be considered almost independent. Thus, we can assume that as the frequency increases the G΄will have the same value with the value at ω = 100 rad/sec.

The following figure (Figure 21) depicts the speed of sound as function of G´ at frequency ω = 100 rad/sec.

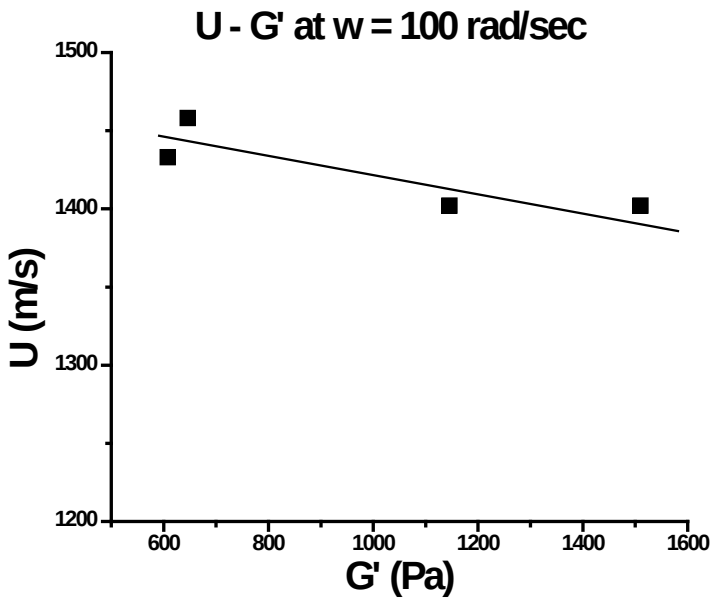

Figure 21: U as function G´ at ω=100 rad/sec of sample with different concentration of softener.

From Figure 21, we observe that the higher the G´ value ,the lower the speed of sound. So, we conclude in the same result with the photoacoustic measurements. More specifically, the speed of sound reduces when increasing the concentration of softener.

VI. Conclusion and Future Work

The aim of this thesis was to manufacture 3D phantoms with tissue-like optical and mechanical properties, using PVCP as main material and adding colors which absorb in visible and infrared spectrum and softener in order to change the mechanical properties as well the speed of sound.

For the characterization of the optical properties, spectrophotometer measurements were performed which informed us about the absorption spectrum of each specimen.

More specially, we observed that the PVCP absorb at wavelengths 910, 1190 and 1400nm, which can be considered as a characteristic behavior of this material. This behavior was present in all samples, but the spectrum changed only when a color was added as PVCP itself does not absorb.

Furthermore, the speed of sound was defined by using the photoacoustic effect. This method informs us about the time required for the photoacoustic signal to propagate from the bottom of the sample until it is detected from the ultrasound transducer placed on its upper surface. However, to define the speed of sound, the thickness of the sample is necessary. Due to the fact that the PVCP samples are very soft and present huge deformation, thickness measurements were performed by using an optical microscope by focusing on the upper and the bottom surface of specimen. However, the measurement process of calculating the speed of sound presented abig error propagation. It was also observed that the speed of sound decreased as the concentration of softener increased.

Finally, the characterization of mechanical properties was performed by rheometer use. From these measurements, we understand that the PVCP samples are solid -like as G´ (Elastic modulus) is bigger than G´´(viscosity term) and G´can be considered steady in higher frequencies (more than 100 rad/sec). Moreover, we observed that the G´term was reduced as softener concentration increased.

Finally we concluded to the same result by performing both photoacoustic and rheological measurements as well. As the softener concentration increases, the G´ reduces but the speed of sound tends to increase. A first assumption for the reason why this phenomenon is observed could be due to the fact that the photoacoustic wave prefers to propagate through channels that softener addition creates in the material's structure.

A future step of this work could be the characterization these samples for scattering and the definition of absorption and scattering coefficients. The same process could be done in different compositions of colors and hardness. In addition, a multilayer PVCP phantom could be manufactured as well. Finally, a next step should be the more accurate thickness measurement in order to define the speed of sound with smaller errors.

VII. References

[1] Xu T, Zhang C, Wang X, Zhang L and Tian J 2003 Measurement and analysis of light distribution in Intralipid-10% at 650 nm *Appl. Opt.* **42** 5777–84

[2] Tanaka T 1981 Gels *Sci. Am.* **244** 124–136, 138

[3] Iizuka M N, Sherar M D and Vitkin I A 1999 Optical phantom materials for near infrared laser photocoagulation studies *Lasers Surg. Med.* **25** 159–69

[4] Korte C L, Cespedes E I, van der Steen A F, Norder B and te Nijenhuis K 1997 Elastic and acoustic properties of vessel mimicking material for elasticity imaging *Ultrason. Imaging* **19** 112–26

[5] Pogue B and Patterson2006 Review of tissue simulating phantoms for optical spectroscopy, imaging and dosimetry Journal of biomedical optics **11**041102

[6] Avtzi S 2014*Fabrication and characterization of a 3-d non-homogeneous tissue – like mouse phantom for optical imaging Biophotonics* p. 49

[7] Firbank M, Oda M and Delpy D 1995 An improved design for a stable and reproducible phantommaterial for use in near-infrared spectroscopy and imagingPhys. Med. Biol.**40** 955–61

[8] Kharine, A., Manohar, S., Seeton, R., Kolkman, R. G. M., Bolt, R. A., Steenbergen, W., and de Mul, F. F. M., Poly(vinyl alcohol) gels for use as tissue phantoms in photoacoustic mammography.," Phys Med Biol 48(3), 357{70 (2003)

[9] Henrichs P M, Meador J, Mehta K, Miller T, Yee A and Oraevsky A A 2004 Phantoms for development of LOISTM as a modality for diagnostic imaging of breast cancer Proc. SPIE 5320 8–15

[10] Spirou, G. M., Oraevsky, A. A., Vitkin, I. A., and Whelan, W. M., \Optical and acoustic properties at 1064 nm of polyvinyl chloride-plastisol for use as a tissue phantom in biomedical optoacoustics," Physics in Medicine and Biology 50(14), N141{53 (2005)

[11] Fonseca Martina Characterisation of a PVCP-based tissue-mimicking phantom for quantitative photoacoustic imaging

[12] Lorenzo, J.R. and ebrary Inc., Principles of diffuse light propagation light propagation in tissues with applications in biology and medicine. 2012, World Scientific Pub. Co.,: Singapore. p. xvii, 336 p. ill.

[13] Second window for in vivo imaging, Andrew M. Smith, Michael C. Mancini, and Shuming Nie

[14] Ntziachristos, V., Going deeper than microscopy: the optical imaging frontier in biology. Nat Methods, 2010. 7(8): p. 603-14.

[15] Photoacoustic imaging in biomedicine

[16] Li, C. & Wang, L. V. Photoacoustic tomography and sensing in biomedicine. Physics in medicine and biology 54, R59-97, doi:10.1088/0031-9155/54/19/R01 (2009).

[17] Tserevelakis, G. J., Tsagkaraki, M. & Zacharakis, G. Hybrid photoacoustic and optical imaging of pigments in vegetative tissues. J Microsc 263, 300-306,

[18] Chapter 2 Mechanical Properties of Biological Materials S. Pal, Design of Artifi cial Human Joints & Organs DOI 10.1007/978-1-4614-6255-2_2, © Springer Science+Business Media New York 2014

[19] Oscillatory Rheology Measuring the Viscoelastic Behaviour of Soft Materials

[20] http://ws.eastman.com/ProductCatalogApps/PageControllers/ProdDatasheet_PC.aspx?product=71066420
[21] Van de Ven, J. D. and Erdman, A. G., \Near-infrared laser absorption of poly(vinyl chloride) at elevated temperatures," Journal of Vinyl and Additive Technology 12(4), 166{173 (2006)
[22] Bohndiek, S. E., Bodapati, S., Van De Sompel, D., Kothapalli, S.-R., and Gambhir, S. S., \Development and application of stable phantoms for the evaluation of photoacoustic imaging instruments.," PloS one 8(9), e75533 (2013).

VIII. Ευχαριστίες

Η παρούσα διπλωματική εργασία εκπονήθηκε στο εργαστήριο In Vivo Imaging Lab του Ινστιτούτου Ηλεκτρονικής Δομής και Λέιζερ (Ι.Η.Δ.Λ) του Ι.Τ.Ε στα πλαίσια της διπλωματικής μου εργασίας στο Τμήμα Φυσικής. Η ολοκλήρωση αυτής της εργασίας σημαίνει τη λήξη μιας σημαντικής περιόδου για μένα και είναι αποτέλεσμα προσωπικής αλλά και συλλογικής δουλειάς. Για το λόγο αυτό θα ήθελα να ευχαριστήσω τους παρακάτω ανθρώπους που με βοήθησαν στη διεκπεραίωση αυτής της πτυχιακής.

Κατ' αρχάς, θα ήθελα να ευχαριστήσω τον δρ, κ. Γιάννη Ζαχαράκη που μου έδωσε την ευκαιρία να εργαστώ σε αυτό το εργαστήριο και να ανακαλύψω πολύ ενδιαφέροντα πράγματα.

Ένα μεγάλο ευχαριστώ στην Στέλλα Αβτζή για την συμπαράσταση, βοήθεια, συμβουλές και καθοδήγηση για ό, τι και αν προέκυπτε όλον αυτόν τον καιρό.

Επίσης θα ήθελα να ευχαριστήσω τον δρ. Γιώργο Τσερεβελάκη, ο οποίος είναι εκείνος που ανέπτυξε την πειραματική διάταξη για το φωτοακουστικό φαινόμενο και για τις συμβουλές μου έδωσε παρ' όλου που συνεργαστήκαμε ελάχιστο χρόνο.

Ευχαριστώ από το βάθη της καρδιάς μου τον κ. Λάμπρο Παπουτσάκη για την συνδεσμολογία για την προετοιμασία των δειγμάτων καθώς και την βοήθεια του όλον αυτό τον καιρό.

Θα ήθελα να ευχαριστήσω τον δρ. κ. Μανώλη Γλυνό για τη συνεργασία και τη μέτρηση των ρεολογικών μετρήσεων.

Επιπλέον θα ήθελα να ευχαριστήσω κάθε μέλος του εργαστηρίου IVIL για την συνεργασία καθώς δημιούργησαν ένα πολύ ευχάριστο και φιλικό κλίμα.

Τέλος, θα ήθελα να ευχαριστήσω την οικογένεια μου για την υποστήριξη, εμπιστοσύνη και ενθάρρυνση που μου παρέχουν σε κάθε δύσκολη στιγμή καθώς και τους φίλους μου που με συμβούλεψαν και ενθάρρυναν τις στιγμές που τους χρειαζόμουν.